

We are IntechOpen, the world's leading publisher of Open Access books Built by scientists, for scientists

4,800

Open access books available

122,000

International authors and editors

135M

Downloads

Our authors are among the

154

Countries delivered to

TOP 1%

most cited scientists

12.2%

Contributors from top 500 universities



WEB OF SCIENCE™

Selection of our books indexed in the Book Citation Index
in Web of Science™ Core Collection (BKCI)

Interested in publishing with us?
Contact book.department@intechopen.com

Numbers displayed above are based on latest data collected.

For more information visit www.intechopen.com



Numerical Analysis and Simulation of Fluidics in Nanogap-Embedded Separated Double-Gate Field Effect Transistor for Biosensor

Maesoon Im^{1,*} and Yang-Kyu Choi²

¹University of Michigan, Ann Arbor

²Korea Advanced Institute of Science and Technology (KAIST)

¹United States of America

²Republic of Korea

1. Introduction

For detection of diverse biomolecules, researchers have developed a wide variety of biosensors, using, for example, fluorescent imaging (Oh et al., 2005), piezoelectric properties (Yang et al., 2006), nano-mechanical properties (Fritz et al., 2000), electrochemical properties (Drummond et al., 2003), conducting properties (Reed et al., 1997; Cui et al., 2001; Patolsky et al., 2007), and so on. Although some of these techniques show ultra-high sensitivity, they require labelling processes for analytes or bulky and expensive equipment for measurement. Label-free detection without necessity of an external apparatus is important in point-of-care testing (POCT) devices (Kost et al., 1999; St-Louis 2000; Tierney et al., 2000), which enable fast and easy on-site detection of biomolecules for health monitoring.

In terms of integration with peripheral CMOS circuitry for realizing a more affordable POCT system, biosensors based on a field-effect transistor (FET) scheme have notable advantages (Schöning & Poghossian, 2002). Hence, FET-based biosensors have been actively studied (Begveld, 2003; Schöning & Poghossian, 2002) since the first report of an ion-sensitive solid-state device (Begveld, 1970). In most FET-based biosensor devices (Schöning & Poghossian, 2002; Kim et al., 2006; Sakata et al., 2007), variation of threshold voltage on a scale of tens of mV was obtained in the detection of biomolecules, and the fabrication process was not fully compatible with conventional CMOS technology. Recently, our group reported a new concept for a FET-based biosensor utilizing dielectric constant change inside nanogaps embedded in a FET device (Im, H. et al., 2007).

In our previous work (Im et al., 2011), we successfully detected the antigen and antibody of avian influenza (AI), which can cause human fatality. Avian influenza antigen (AIa) and antibody (anti-AI) showed a large degree of signal change (*i.e.* a high signal-to-noise ratio) with a fabricated nanogap-embedded separated double-gate field effect transistor (hereafter referred to as “nanogap-DGFET”), shown in Fig. 1 (Im et al., 2011). Fig. 2 shows scanning

* M. Im was with the Department of Electrical Engineering, KAIST, Daejeon 305-701, Republic of Korea. He is now with the Department of Electrical Engineering and Computer Science, University of Michigan, Ann Arbor, MI 48109 USA.

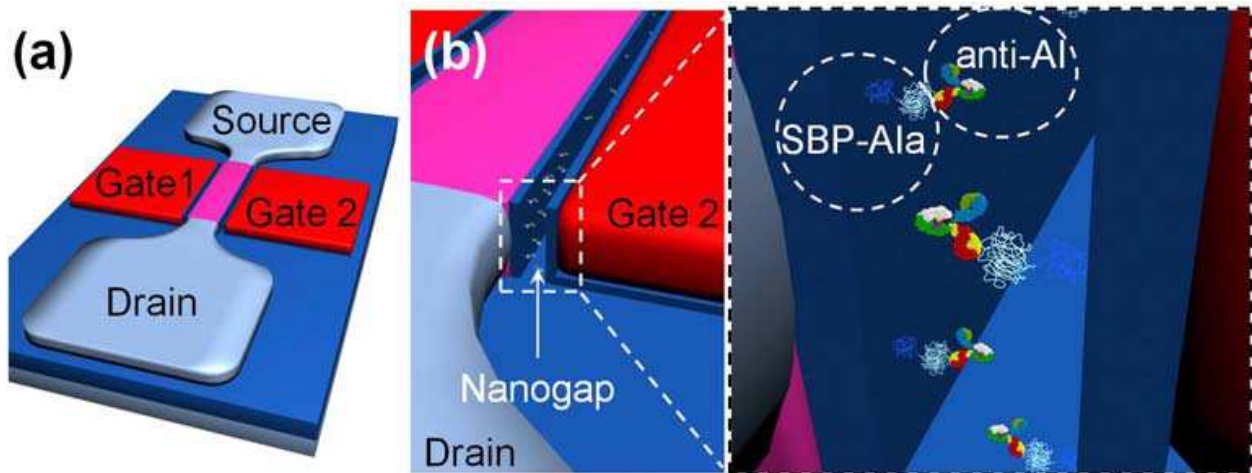


Fig. 1. (a) Schematic diagram of a nanogap-embedded separated double-gate field effect transistor (nanogap-DGFET). (b) Magnified view of the nanogap near the drain and gate 2. Dotted box conceptually shows immobilized avian influenza antigen conjugated with silica binding protein (SBP-Ala) (Gu et al., 2009) and avian influenza antibody (anti-AI) inside the nanogap. Reprinted with permission from (Im et al., 2011) © Copyright 2011 IEEE.

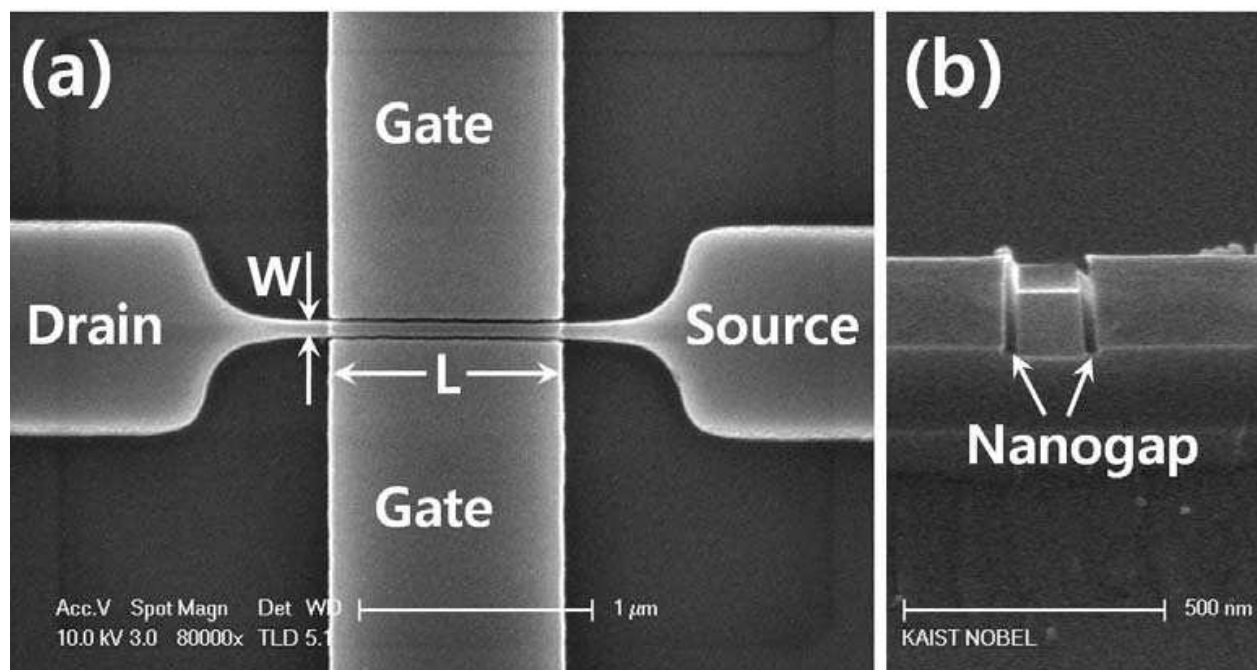


Fig. 2. Scanning electron microscopy images of the fabricated device. (a) Top view of nanogap-embedded separated double-gate field effect transistor. The width (W) and the length (L) of this transistor are 150 nm and 1 μm , respectively. (b) Cross-sectional view of a nanogap in test pattern. The width of nanogap is 30 nm.

electron microscopy (SEM) images of the fabricated nanogap-DGFET device. Large signal change is a desirable feature in a handheld size apparatus for POCT application (Tierney et al., 2000). Moreover, the electrical signal of the nanogap-DGFET biosensor does not depend on the Debye length (Siu & Cobbold, 1979), which is a function of the ionic strength of the sample solution (Schöning & Poghossian, 2002). This is because the nanogap-DGFET devices

are measured in a quasi-dry state, and the detection principle is based on the permittivity change rather than charge effect of biomolecules. On the other hand, the electrical signal of FET biosensors changes significantly with the ionic concentration of the sample solution (Stern et al., 2007). For general POCT application, it is not easy to control the ionic concentration precisely with any real human sample, such as blood serum, urine, or saliva. Therefore, this feature of Debye-screening-free sensing is another advantage of the nanogap-DGFET, together with moderate sensitivity and large signal change (Im, H. et al., 2007; Gu et al., 2009).

In studies of nanogap-based biosensors (Haguet et al., 2004; Yi et al., 2005), it is very important to understand the fluidics in the nanogap (Brinkmann et al., 2006) because most biomolecules are immobilized and coupled inside a nanogap immersed in a water-based solution. In order to examine the fluidic characteristics in the nanogap of nanogap-DGFET devices, theoretical calculations and numerical simulations are performed in this study. Three-dimensional simulation results dynamically visualize the process of liquid filling the nanogap.

2. Fluidics in the nanogap of the nanogap-DGFET

The mechanism by which the nanogap is filled with the sample solution is an important aspect of the nanogap-DGFET. In the wet etching process of the nanogap, the liquid fills the nanogap by chemically-assisted injection of liquid, *i.e.* the nanogap is filled with a diluted fluoric acid solution while being etched (Im et al., 2011). The SEM image in Fig. 2(b) clearly shows the resultant nanogap structure from wet etching. However, in real experiments for the detection of biomolecules, the sample solution containing analytes should enter the nanogap for immobilization of biomolecules such as DNAs, antibodies, antigens, and so on. If the nanogap cannot be wetted by the sample solution, the nanogap-DGFET cannot be used as a biosensor. Filling the nanogap with the solution presents challenges, as the gap is initially filled with air before applying the sample solution and is in a nanometre dimension, and thus the surface tension of the liquid has significant effects.

As performed in a previous work (Brinkmann et al., 2006), it is worthwhile to estimate the fluidic properties inside the nanogap of the nanogap-DGFET with a simplified model and theoretical calculations before three-dimensional simulation results are discussed.

2.1 Capillary pressure in the nanogap

The liquid is expected to be injected by capillary force rather than by gravity into the nanogap of the nanogap-DGFET owing to the nanometre scale of the gap. Therefore, capillary pressure inside the nanogap is an essential aspect of the fluidic behaviour of the sample solution that will be loaded in the nanogap. This section discusses modelling and computation of the capillary pressure inside the nanogap.

Fig. 3 is a schematic illustration showing notations of symbols used in the modelling and calculation. The sample solution in the nanogap can be modelled as shown in Fig. 4. It is apparent that the entire region except for the nanogap will become wet immediately after introduction of the sample liquid on top of the device, because the exposed surface of the nanogap-DGFET is a native oxide, which is hydrophilic. If the nanogap is initially filled with air, we can assume that two sidewalls (*i.e.* gate side and channel side) in the nanogap are native oxide and the other two sidewalls are water applied to the system. Therefore, the

capillary pressure (ΔP) inside the nanogap (shown in Fig. 4) with the sample solution of water can be expressed as the following equation (Im, M. et al., 2007):

$$\Delta P = \frac{2}{G} \gamma \cos \theta_{SiO_2} + \frac{2}{L} \gamma \cos \theta_{water} \quad (1)$$

where γ is the liquid surface tension of the sample solution, θ_{SiO_2} is the contact angle of silicon dioxide, θ_{water} is the contact angle of water (full wetting), G is the width of the nanogap, and L is the length of the nanogap, as shown in Fig. 3 and Fig. 4. For the sample solution of water, capillary pressures estimated with Equation (1) are plotted in Fig. 5. In the case of nanogap length of $1\mu\text{m}$, the capillary pressure (ΔP) is about 3.38MPa.

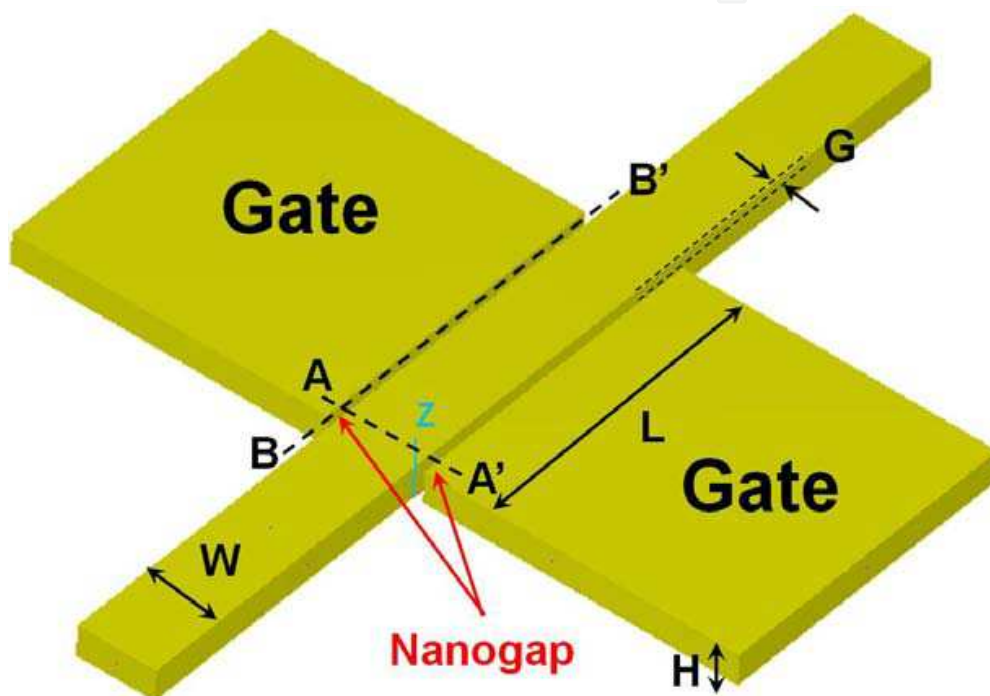


Fig. 3. Schematic diagram showing notation of symbols used in calculations and simulations.

2.2 Theoretical calculation of the nanogap filling depth

The sample solution continues to enter the nanogap if the capillary force is larger than the pressure difference between the pressure inside the nanogap (P_x) and the atmospheric pressure ($P_0=0.1\text{MPa}$). In the worst case where air cannot be evacuated from the nanogap, the pressure inside the nanogap will be increased by compressed air and will have a relationship delineated as follows:

$$P_x = P_0 \times \frac{H}{H - x} \quad (2)$$

where H is the height of the nanogap. Since the water meniscus will stop at the condition of $\Delta P = P_x - P_0$, we can calculate that the water meniscus can move to $x=97\text{nm}$ of a 100-nm -deep nanogap ($H=100\text{nm}$) even in the worst case, *i.e.* the nanogap is filled with compressed air.

This calculation result means that capillary pressure is sufficient to deliver the water to the bottom surface of the nanogap. We will confirm this result with three-dimensional simulations in the following section.

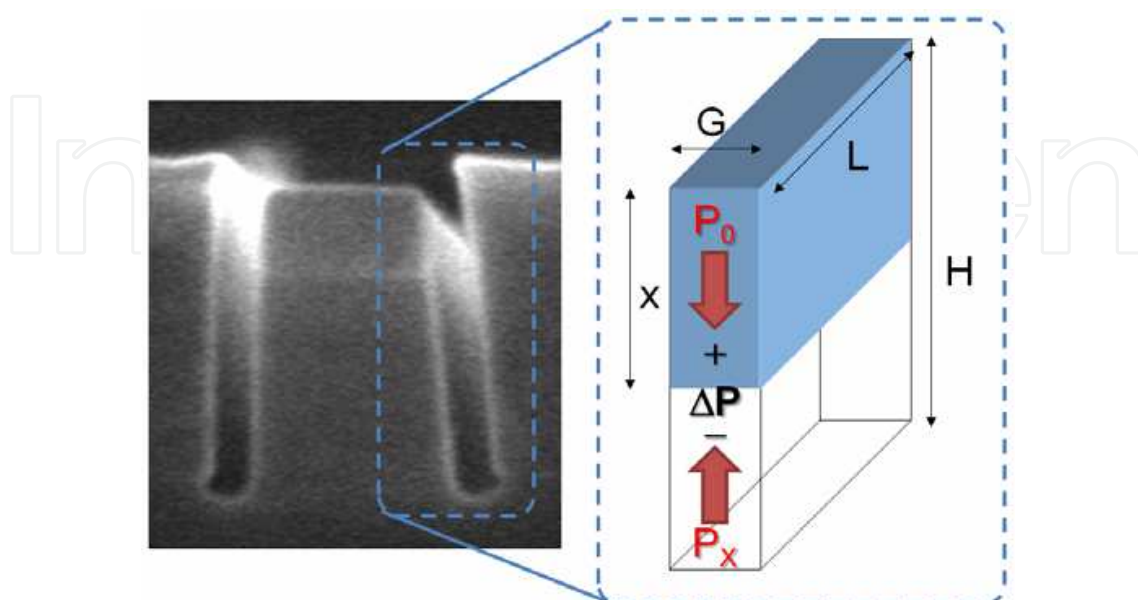


Fig. 4. A capillary force modeling of the nanogap highlighted by the dotted box in the SEM image displaying AA' direction as shown in Fig. 3. G is the nanogap width, L is the nanogap length, H is the nanogap height, x is the water penetration depth, P_0 is the atmospheric pressure, P_x is the pressure inside the nanogap, and ΔP is the pressure difference between P_x and P_0 .

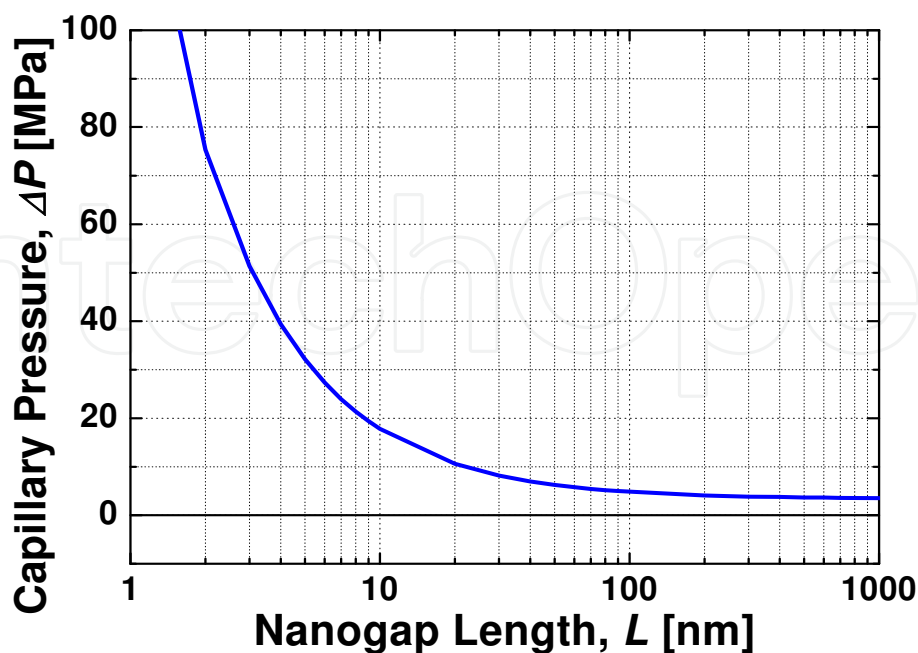


Fig. 5. A plot of capillary pressures as a function of the nanogap length, where $G=30\text{nm}$, $\theta_{\text{SiO}_2}=45^\circ$, $\theta_{\text{water}}=0^\circ$, and $\gamma=72.5\text{mN/m}$ for the sample solution of water.

3. Numerical simulations of the nanogap filling process

Although a study on the fluidics on a nanogap was previously carried out (Brinkmann et al., 2006) to support earlier results with a nanogap biosensor (Haguet et al., 2004), only theoretical calculations were presented. In order to visualize the nanogap filling and support the calculation results provided in previous section, three-dimensional simulations were also performed using CFD-ACE+™ (CFD Research Corporation, Huntsville, Alabama, USA) with the structure shown in the inset of Fig. 3. CFD-ACE+™ is a commercial software for multiphysics simulation, and has been used in previous microfluidic studies (Jen et al., 2003; Kobayashi et al., 2004; Rawool et al., 2006; Rawool & Mitra, 2006; Yang et al., 2007; Im et al., 2009).

3.1 Simulation setup

The finite element method is applied with structured grids, as shown in Fig. 6. In order to observe the fluidic behaviour in nanogaps, fine meshes are used in the nanogaps, as highlighted by the red dotted box in Fig. 6. On top of the nanogap-DGFET structure shown in Fig. 3, 1.5- μm -high regions are additionally assigned for an initial water position mimicking introduction of a water droplet on the nanogap-DGFET. The total number of cells is 205,760 in 28 structured zones. Flow and Free Surfaces (VOF) modules are used in this simulation. In the VOF module, the surface reconstruction method is chosen to be 2nd Order (PLIC), and surface tension is considered. The wetting angle of the sidewall in the nanogaps is assumed to be 45 deg due to the presence of native oxide. In addition to surface tension, gravitational force is also considered along the Z-direction, as shown in Fig. 3. The reference pressure of 100,000 N/m² (0.1 MPa) is set as the atmospheric pressure. Table 1 summarizes the physical properties of water used in this simulation study.

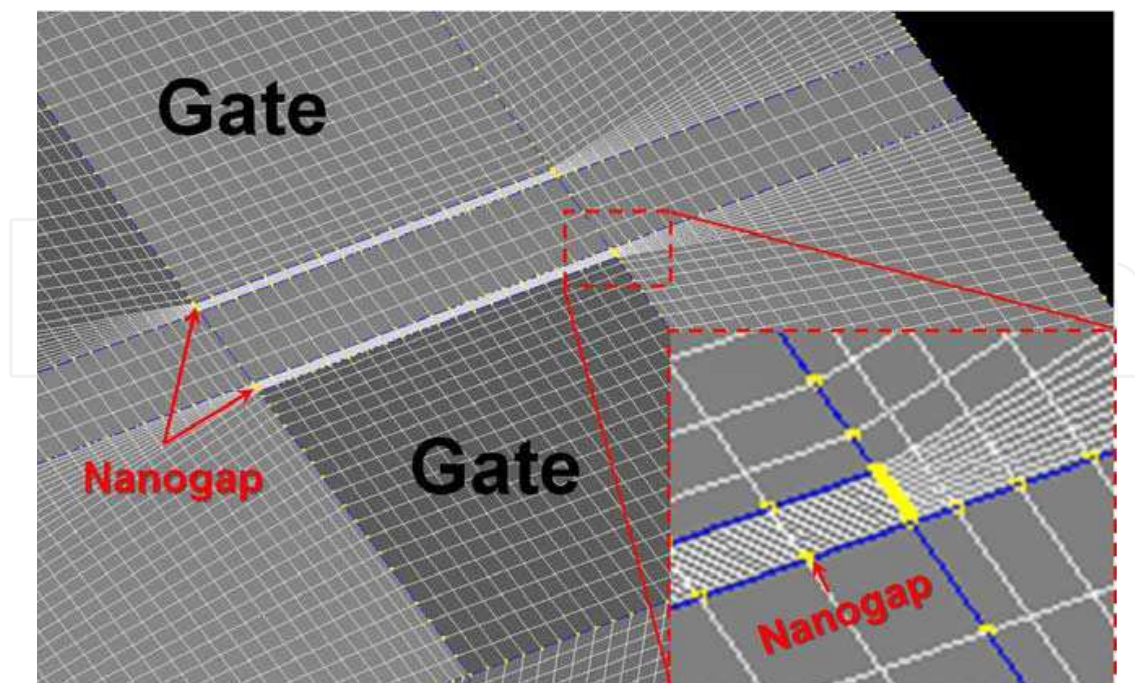


Fig. 6. Grid shapes for structured meshes for simulation. The dotted red box shows fine meshes in the nanogap region.

Physical property	Value	Comment
Density (kg/m ³)	1000	Constant
Viscosity (m ² /s)	1×10 ⁻⁶	Constant (Kinematic)
Surface tension (N/m)	0.0725	Constant

Table 1. Properties of water in the numerical simulation

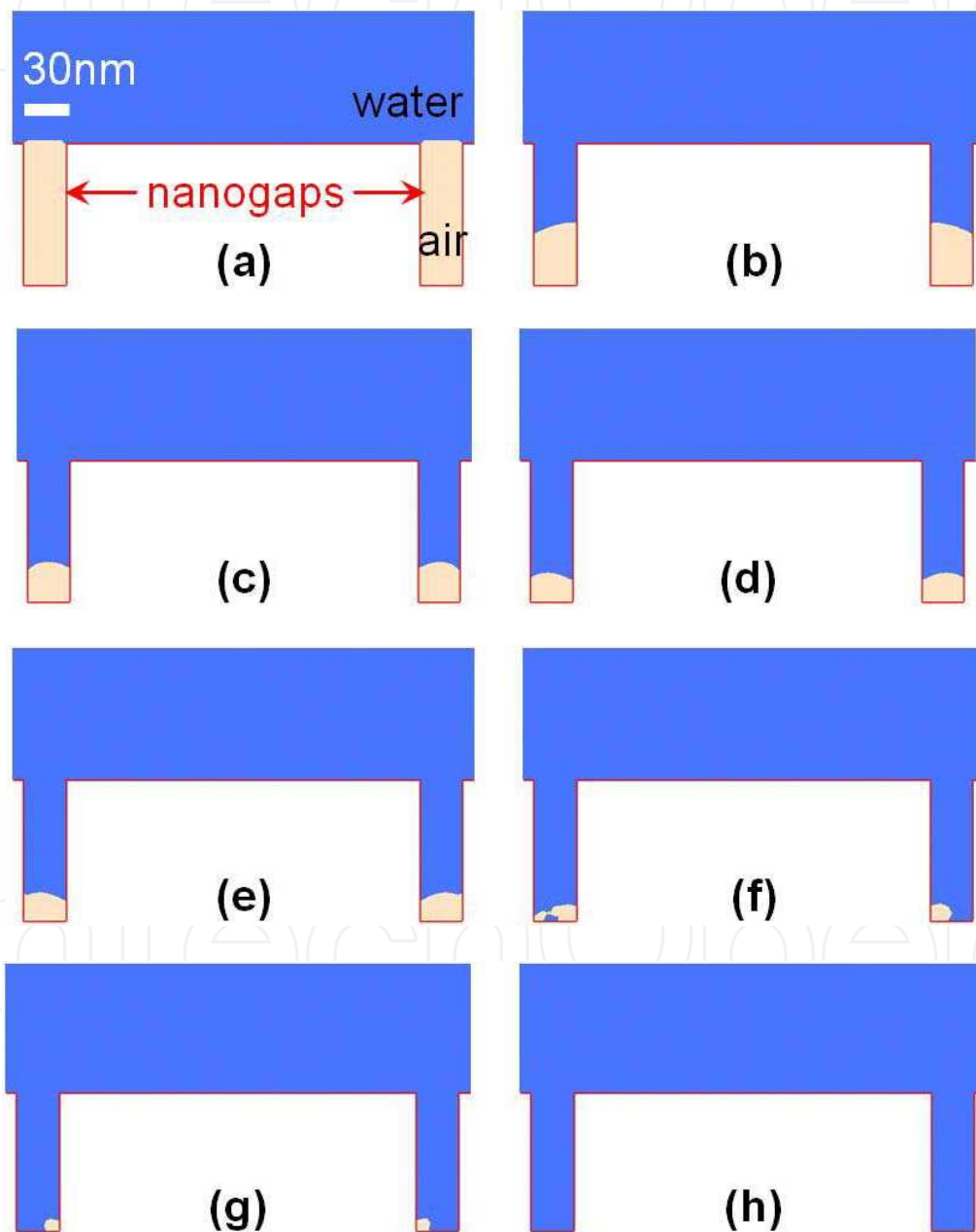


Fig. 7. Nanogap filling of the sample solution of water at the nanogap edge indicated as AA' in Fig. 5. At various instants of (a) 0 nsec (Initially, air is in the nanogap) (b) 95 nsec (c) 163 nsec (d) 315 nsec (e) 573 nsec (f) 643 nsec (g) 650 nsec (h) 681 nsec (Finally, the nanogap is filled with the sample solution)

3.2 Simulation results: nanogap filling

Fig. 7 shows the water meniscus positions at various instants from the nanogap edge which is denoted as AA' in Fig. 3. Air inside the nanogap is continuously squeezed and compressed by marching water along the sidewalls of the nanogap. Finally, the entire region of the nanogap becomes filled with water, as confirmed in Fig. 7(h).

It is noteworthy that the wetting speeds are different at the centre and at the edge of the nanogap in the simulation results. Positions of the water meniscus are plotted in Fig. 8; the nanogap is completely filled with water within 700 nsec at the edge of the nanogap; however, it takes longer than that at the centre of the nanogap.

From the calculation results in the previous section and the simulation results in this section, we can find an interesting aspect of the fluidics in the nanogap. The length of the nanogap is effectively reduced after some portion of the nanogap is wetted, because wetting occurs from the edge of the nanogap. With a shorter nanogap, it is straightforward that the capillary pressure becomes greater, as shown in Fig. 5. As a consequence, we can conclude that the nanogap can be fully wetted with the sample solution by this sort of positive feedback.

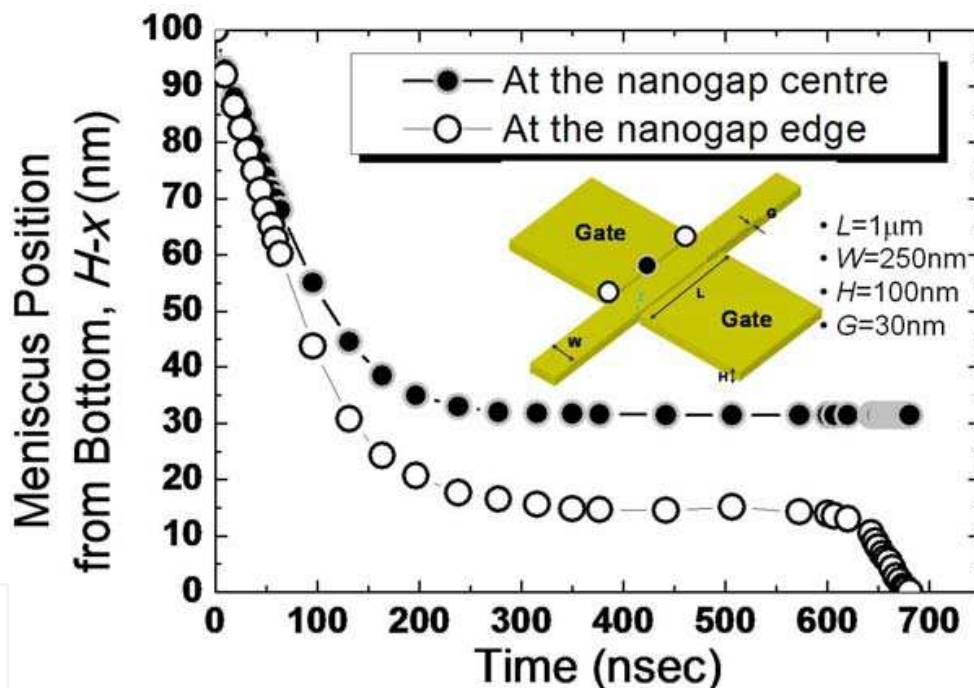


Fig. 8. Water meniscus positions as a function of time in the simulation structure shown in the inset ($L=1\mu\text{m}$, $W=250\text{nm}$, $H=100\text{nm}$, and $G=30\text{nm}$). Hollow circles mean meniscus positions at the nanogap edge and solid circles mean meniscus positions at the nanogap centre.

The plateau in the graph of Fig. 8 is attributed to the pressure of the compressed air being too high for the capillary pressure to overcome for further advancement. This phenomenon is confirmed by monitoring pressure changes inside the nanogap together with corresponding water meniscus positions. As shown by the dotted boxes in Fig. 9, the pressure inside the nanogap increases gradually as the meniscus advances to the bottom of the nanogap. In the process of nanogap filling, there is a period where only pressure increment is observed without meaningful progress of the water meniscus locations.

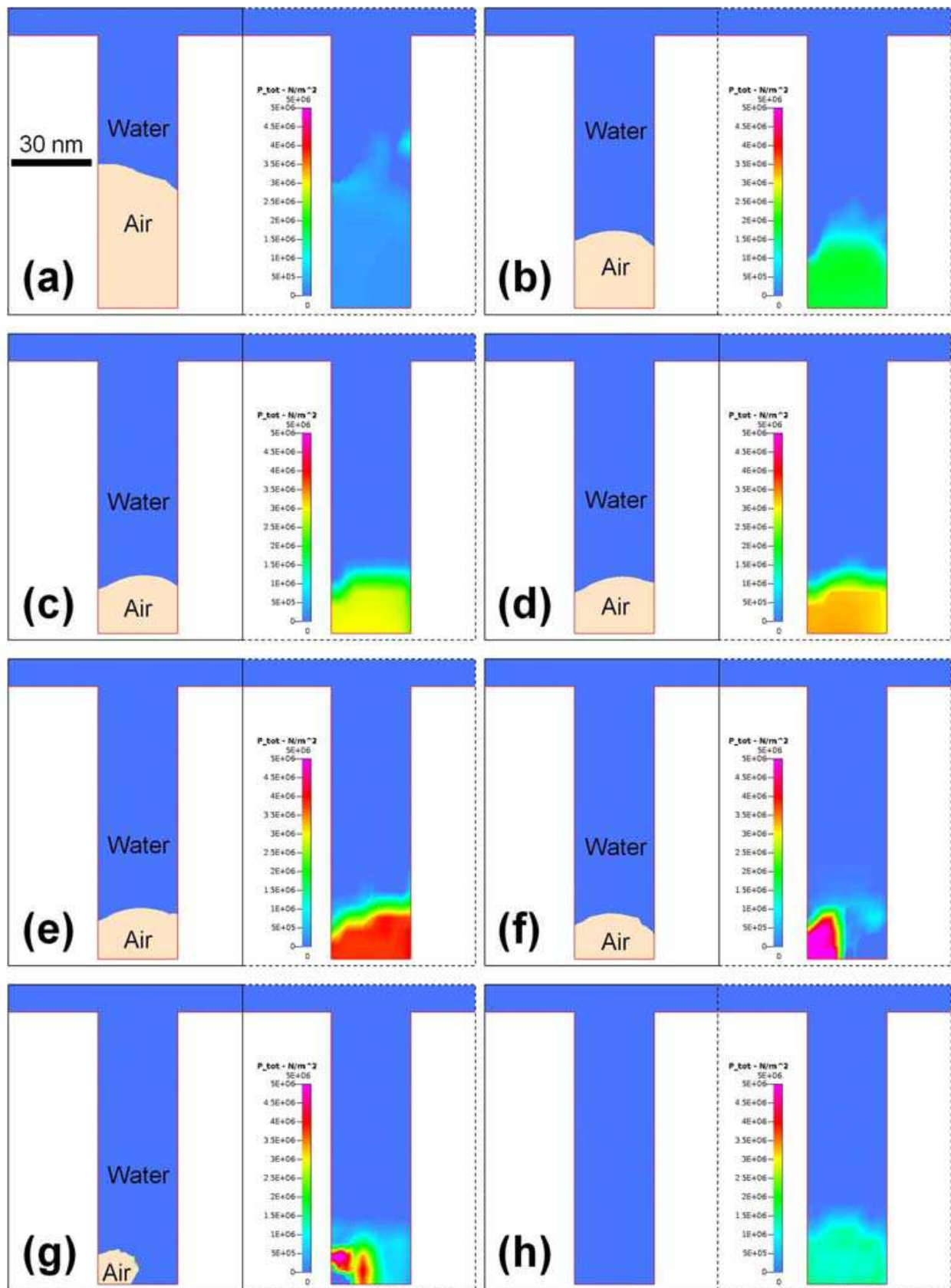


Fig. 9. Water meniscus positions (shown in solid boxes) in the nanogap with corresponding pressure changes (shown in dotted boxes).

3.3 Simulation results: expelling air bubbles from the nanogap

As shown in Fig. 9, air trapped inside the nanogap is pressurized by the capillary pressure of water above the air. Then, where does the air finally go? By careful observation of the simulation results, we can see air bubbles appear and disappear repeatedly inside the nanogap, as shown in Fig. 10.

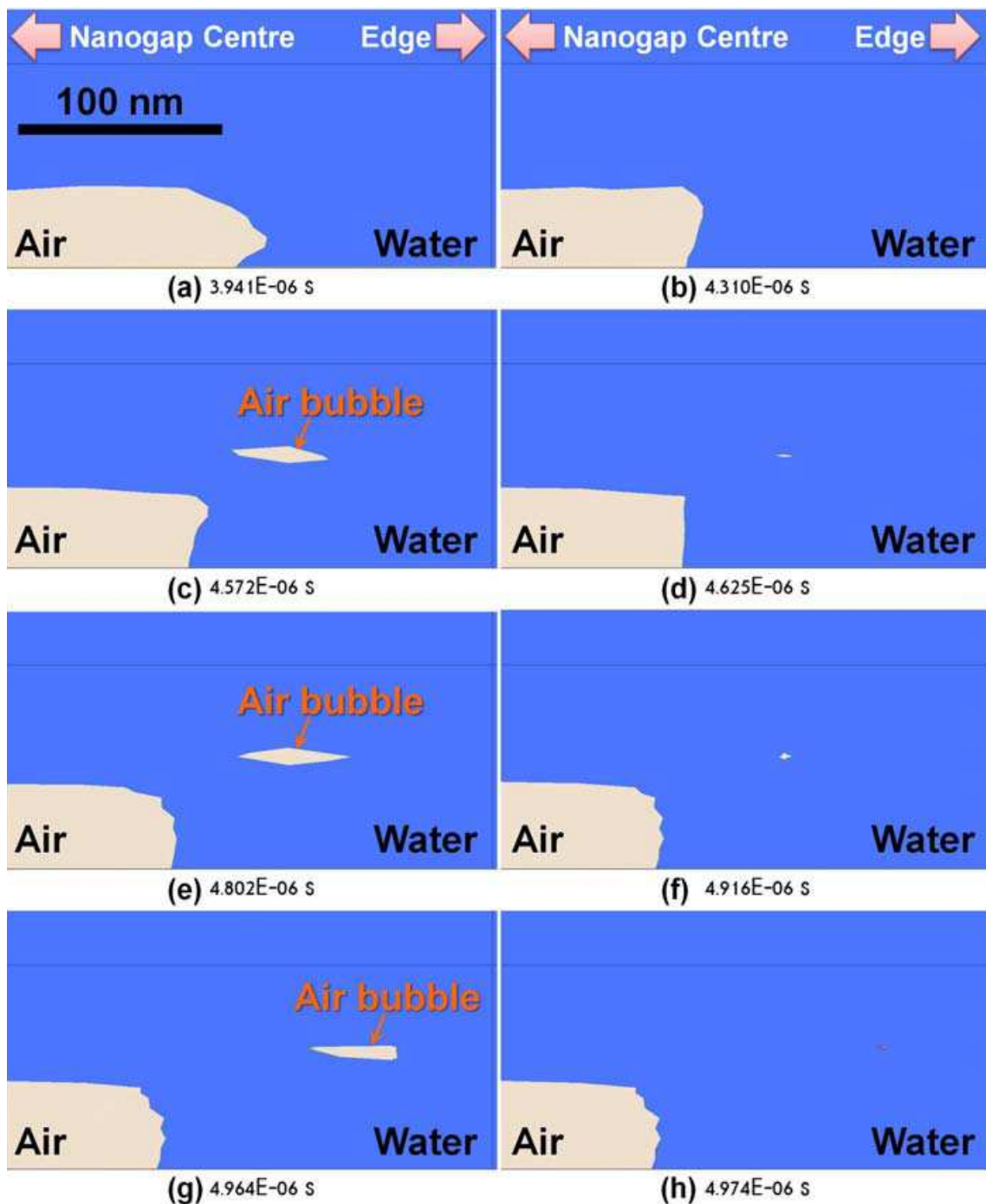


Fig. 10. Movement of water meniscus in the direction of BB' shown in Fig. 5. (Closed-up views near the B' side) (a) 3.941 μsec (b) 4.310 μsec (c) 4.572 μsec (d) 4.625 μsec (e) 4.802 μsec (f) 4.916 μsec (g) 4.964 μsec (h) 4.974 μsec . Air bubbles appears and disappears repeatedly to lower the pressure of the air trapped inside the nanogap.

Because water continuously compresses the air in the nanogap with capillary pressure, it is analyzed that a certain threshold pressure is necessary for the trapped air to evacuate an air bubble against the capillary pressure. After the appearance of air bubbles, which occurs with reduced pressure of the trapped air, the water meniscus proceeds further toward the nanogap centre by additional compression of trapped air. Generated air bubbles from the trapped air last for a period of a few tens of nanoseconds to three hundreds nanoseconds. By repetition of this process (*i.e.* pressure reduction by air bubbles and further compression), the nanogap is gradually filled with water.

From the simulation, the threshold pressure for generation of air bubbles is estimated to be around 5MPa, which is 50 times the atmospheric pressure (0.1MPa). As shown in Figs. 9(f) through 9(h), trapped air is eliminated after the pressure reaches roughly 5MPa. Air bubbles cannot be seen in Fig. 9, because they will appear in different places, as shown in Fig. 10.

3.4 Simulation results: velocity vectors

The blue arrows in Fig. 11 represent velocity vectors of water and air in designated meshes. These velocity vectors are obtained from the plane 5 nm away from the nanogap edge, as shown in the figure. In the initial stage of nanogap filling, as shown in Fig. 11(a), air exits quickly from the nanogap by advancing water. After velocity reduction of air, as seen in Fig. 11(b), the velocity direction of air changes toward the nanogap centre in the stage of compressing air, as shown in Fig. 11(c). Finally, if some plane is filled with water, water will fill the trapped air region at the nanogap centre, and consequently the velocity vectors are oriented toward the centre of the nanogap, as shown in Fig. 11(d).

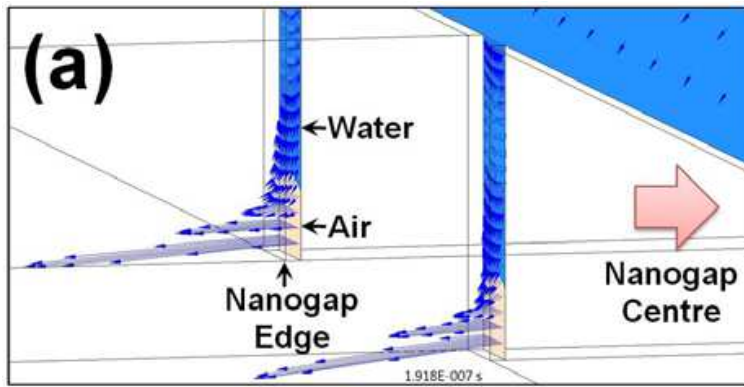
Fig. 12 shows velocity vectors when water cannot advance because compressed air resists against the water. It is shown that the velocity vectors are oriented upward at the water/air interface due to high pressure, represented by green colour in Fig. 12(b), which indicates pressure of around 2MPa.

4. Conclusions

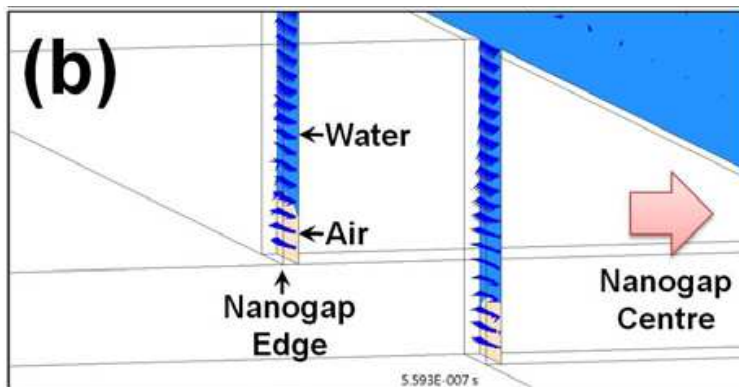
In this chapter, nanogap-DGFET's fluidic characteristics are discussed with theoretical calculations as well as numerical simulations. Theoretical computation based on appropriate modelling predicts that almost complete filling of the nanogap with water is possible. Three-dimensional simulations using CFD-ACE+TM support the theoretical calculations. Various characteristics such as water meniscus position, pressure distribution, and velocity vectors in the simulation results have been analyzed in detail for comprehensive understanding of the process of nanogap filling in the nanogap-embedded biosensor. The sample solution of water is expected to completely fill the nanogap by capillary pressure. These results indicate that biomolecules in a water-based sample solution can be successfully delivered to sensing regions (*i.e.* nanogaps) in nanogap-DGFET devices.

5. Acknowledgment

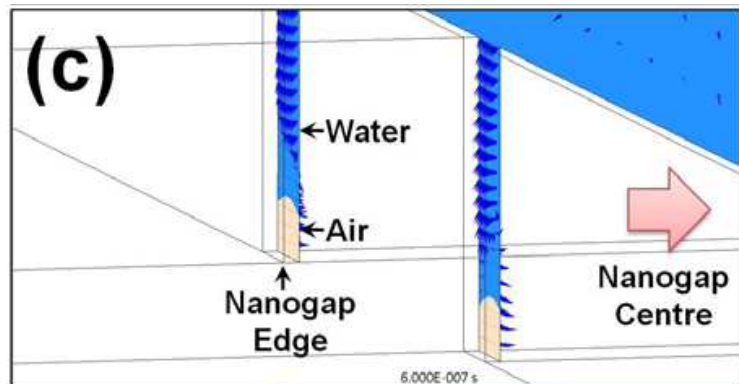
This work was supported in part by a National Research Foundation of Korea (NRF) grant funded by the Korean Ministry of Education, Science and Technology (MEST) (No. 2010-0018931), in part by the National Research and Development Program (NRDP, 2010-0002108) for the development of biomedical function monitoring biosensors, which is also



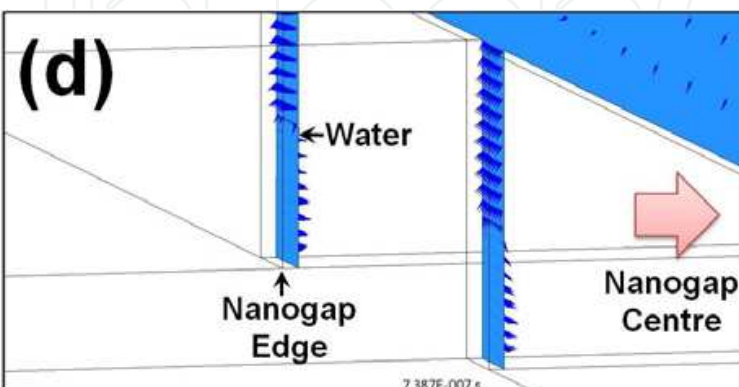
(a) 191.8 nsec after beginning of water penetration, air exits with fast velocity from the nanogap by capillary force of water from the top. Velocity vectors of water are toward the bottom of the nanogap.



(b) 559.3 nsec after beginning of water penetration, air still exits with reduced velocity from the nanogap. Water is being supplied from the top of the nanogap.



(c) 600.0 nsec after beginning of water penetration, the direction of air velocity vectors is changed toward the nanogap centre due to additional capillary force from the nanogap edge which is completely filled with water. As shown in Fig. 8, the nanogap edges become wet before the nanogap centre does.



(d) 738.7 nsec after beginning of water penetration, water at the lower part of nanogap moves to the nanogap centre to fill the remainder of the nanogap at this region, as described in Fig. 10.

Fig. 11. Distribution of velocity vectors (shown as blue arrows) of air and water at 5 nm away from a nanogap edge.

funded by the Korean Ministry of Education, Science and Technology. The work of M. Im was supported in part by the Brain Korea 21 Project, the School of Information Technology, KAIST, 2009. The authors would like to thank Mr. Jae-Hyuk Ahn, Dr. Jin-Woo Han, Dr. Tae Jung Park, and Prof. Sang Yup Lee for their help in the fabrication and analysis of real nanogap-DGFET devices in a previous study that motivated this work.

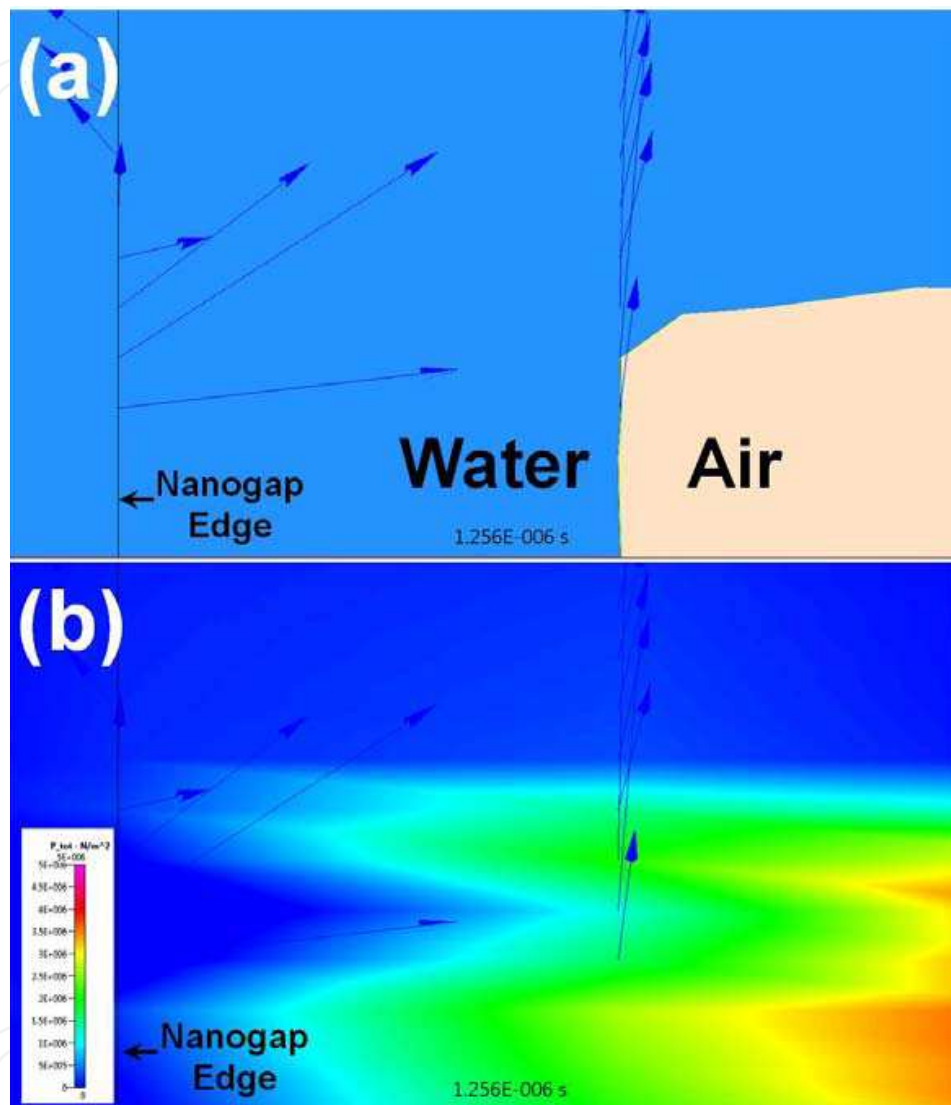


Fig. 12. Velocity vectors in the direction of BB' shown in Fig. 5 with (a) water/air boundary and (b) pressure distribution.

6. References

- Bergveld, P. Development of an ion-sensitive solid-state device for neurophysiological measurements. *IEEE Transactions on Biomedical Engineering*, Vol. BME-17, No. 1, (January 1970), pp. 70-71, ISSN 0018-9294.
- Bergveld, P. Thirty years of Isfetology what happend in the past 30 years and what may happen in the next 30 years. *Sensors and Actuators B : Chemical*, Vol. 88, No. 1, (January 2003), pp. 1-20, ISSN 0925-4005.

- Brinkmann, M. ; Blossy, R. ; Marcon, L. ; Stiévenard, D. ; Dufrêne, Y. F. & Melnyk, O. Fluidics of a Nanogap. *Langmuir*, Vol. 22, No. 23, (October 2006), pp. 9784-9788, ISSN 0743-7463.
- Cui, X. D. ; Primak, A. ; Zarate, X. ; Tomfohr, J. ; Sankey, O. F. ; Moor, A. L. ; Moore, T. A. ; Gust, D. ; Harris, G. & Lindsay, S. M. Reproducible measurement of single-molecule conductivity. *Science*, Vol. 294, No. 5542, (October 2001), pp. 571-574, ISSN 0036-8075.
- Drummond, T. G. ; Hill, M. G. & Barton, J. K. Electrochemical DNA sensors. *Nature Biotechnology*, Vol. 21, No. 10, (October 2003), pp. 1192-1199, ISSN 1087-0156.
- Fritz, J. ; Baller, M. K. ; Lang, H. P. ; Rothuizen, H. ; Vettiger, P. ; Meyer, E. ; Güntherodt, H.-J. ; Gerber, Ch. & Gimzewski, J. K. Translating biomolecular recognition into nanomechanics. *Science*, Vol. 288, No. 5464, (April 2000), pp. 316-318, ISSN 0036-8075.
- Gu, B. ; Park, T. J. ; Ahn, J.-H. ; Huang, X.-J. ; Lee, S. Y. & Choi, Y.-K. Nanogap field-effect transistor biosensors for electrical detection of avian influenza. *Small*, Vol. 5, No. 21, (November 2009), pp. 2407-2412, ISSN 1613-6810.
- Haguet, V. ; Martin, D. ; Marcon, L. ; Heim, T. ; Stiévenard, D. ; Olivier, C. ; El-Mahdi, O. & Melnyk, O. Combined nanogap nanoparticles nanosensor for electrical detection of biomolecular interactions between polypeptides. *Applied Physics Letters*, Vol. 84, No. 7, (February 2004), pp. 1213-1215, ISSN 0003-6951.
- Im, H. ; Huang, X.-J. ; Gu, B. & Choi, Y.-K. A dielectric modulated field-effect transistor for biosensing. *Nature Nanotechnology*, Vol. 2, (June 2007), pp. 430-434, ISSN 1748-3387.
- Im, M. ; Cho, I.-J. ; Yun, K.-S. & Yoon, E. Electromagnetic actuation and microchannel engineering of a polymer micropen array integrated with microchannels and sample reservoirs for biological assay patterning. *Applied Physics Letters*, Vol. 91, No. 12, (September 2007), 124101(3pp), ISSN 0003-6951.
- Im, M. ; Im, H. ; Kim, D.-H. ; Lee, J.-H. ; Yoon, J.-B. & Choi, Y.-K. (2009). Analysis of a superhydrophobic microlens array surface : as a microchannel wall for pressure drop reduction, *Proceedings of Thirteenth International Conference on Miniaturized Systems for Chemistry and Life Sciences (μTAS2009)*, pp. 162-164, ISSN 1556-5904, Jeju, South Korea, November 1-5, 2009.
- Im, M. ; Ahn, J.-H. ; Han, J.-W. ; Park, T. J. ; Lee, S. Y. & Choi, Y.-K. Development of a point-of-care testing platform with a nanogap-embedded separated double-gate field effect transistor array and its readout system for detection of avian influenza. *IEEE Sensors Journal*, Vol. 11, No. 2, (February 2011), pp. 351-360, ISSN 1530-437X.
- Jen, C.-P. ; Wu, C.-Y. ; Lin, Y.-C. & Wu, C.-Y. Design and simulation of the micromixer with chaotic advection in twisted microchannels. *Lab on a chip*, Vol. 3, (April 2003), pp. 77-81, ISSN 1473-0197.
- Kim, D.-S. ; Park, J.-E. ; Shin, J.-K. ; Kim, P.K. ; Lim, G. & Shoji, S. An extended gate FET-based biosensor integrated with a Si microfluidic channel for detection of protein complexes. *Sensors and Actuators B: Chemical*, Vol. 117, No. 2, (October 2006), pp. 488-494, ISSN 0925-4005.

- Kobayashi, I. ; Mukataka, S. & Nakajima, M. CFD simulation and analysis of emulsion droplet formation from straight-through microchannels. *Langmuir*, Vol. 20, No. 22, (September 2004), pp. 9868-9877, ISSN 0743-7463.
- Kost, G. J. ; Ehrmeyer, S. S. ; Chernow, B. ; Winkelman, J. W. ; Zaloga, G. P. ; Dellinger, R. P. & Shirey, T. The laboratory-clinical interface : point-of-care testing. *Chest*, Vol. 115, No. 4, (April 1999), pp. 1140-1154, ISSN 0012-3692.
- Oh, S. W. ; Moon, J. D. ; Lim, H. J. ; Park, S. Y. ; Kim, T. ; Park, J. B. ; Han, M. H. ; Snyder, M. & Choi, E. Y. Calixarene derivative as a tool for highly sensitive detection and oriented immobilization of proteins in a microarray format through noncovalent molecular interaction. *The FASEB Journal*, Vol. 19, No. 10, (August 2005), pp. 1335-1337, ISSN 0892-6638.
- Patolsky, F. ; Timko, B. P. ; Zheng, G. & Lieber, C. M. Nanowire-based nanoelectronic devices in the life sciences. *MRS Bulletin*, Vol. 32, No. 2, (February 2007), pp. 142-149, ISSN 0883-7694.
- Rawool, A. S. ; Mitra, S. K. & Kandlikar, S. G. Numerical simulation of flow through microchannels with designed roughness. *Microfluidics and Nanofluidics*, Vol. 2, No. 3, (February 2006), pp. 215-221, ISSN 1613-4982.
- Rawool, A. S. & Mitra, S. K. Numerical simulation of electroosmotic effect in serpentine channels. *Microfluidics and Nanofluidics*, Vol. 2, No. 3, (February 2006), pp. 261-269, ISSN 1613-4982.
- Reed, M. A. ; Zhou, C. ; Muller, C. J. ; Burgin, T. P. & Tour, J. M. Conductance of a molecular junction. *Science*, Vol. 278, No. 5336, (October 1997), pp. 252-254, ISSN 0036-8075.
- Sakata, T. & Miyahara, Y. Direct transduction of allele-specific primer extension into electrical signal using genetic field effect transistor. *Biosensors and Bioelectronics*, Vol. 22, No. 7, (February 2007), pp. 1311-1316, ISSN 0956-5663.
- Schöning, M. J. & Poghossian, A. Recent advances in biologically sensitive field-effect transistors (BioFETs). *Analyst*, Vol. 127, No. 9, (August 2002), pp. 1137-1151, ISSN 0003-2654.
- Siu, W. M. & Cobbold, R. S. C. Basic properties of the Electrolyte-SiO₂-Si system: physical and theoretical aspects. *IEEE Transactions on Electron Devices*, Vol. ED-26, No. 11, (November 1979), pp. 1805-1815, ISSN 0018-9383.
- Stern, E. ; Wagner, R. ; Sigworth, F. J. ; Breaker, R. ; Fahmy, T. M. & Reed, M. A. Importance of the debye screening length on nanowire field effect transistor sensors. *Nano Letters*, Vol. 7, No. 11, (October 2007), pp. 3405-3409, ISSN 1530-6984.
- St-Louis, P. Status of point-of-care testing : promise, realities, and possibilities. *Clinical Biochemistry*, Vol. 33, No. 6, (August 2000), pp. 427-440, ISSN 0009-9120.
- Tierney, M. J. ; Tamada, J. A. ; Potts, R. O. ; Eastman, R. C. ; Pitzer, K. ; Ackerman, N. R. & Fermi, S. J. The GlucoWatch biographer : a frequent automatic and noninvasive glucose monitor. *Annals of Medicine*, Vol. 32, No. 9, (December 2000), pp. 632-641, ISSN 0785-3890.
- Yang, C.-K. ; Chang, J.-S. ; Chao, S. D. & Wu, K.-C. Two dimensional simulation on immunoassay for a biosensor with applying electrothermal effect. *Applied Physics Letters*, Vol. 91, No. 11, (September 2007), 113904 (3pp), ISSN 0003-6951.

- Yang, Y. T. ; Callegari, C. ; Feng, X. L. ; Ekinici, K. L. & Roukes, M. L. Zeptogram-scale nanomechanical mass sensing. *Nano Letters*, Vol. 6, No. 4, (April 2006), pp. 583-586, ISSN 1530-6984.
- Yi, M. ; Jeong, K.-H. & Lee, L. P. Theoretical and experimental study towards a nanogap dielectric biosensor. *Biosensors and Bioelectronics*, Vol. 20, No. 7, (January 2005), pp. 1320-1326, ISSN 0956-5663.

IntechOpen

IntechOpen



New Perspectives in Biosensors Technology and Applications

Edited by Prof. Pier Andrea Serra

ISBN 978-953-307-448-1

Hard cover, 448 pages

Publisher InTech

Published online 27, July, 2011

Published in print edition July, 2011

A biosensor is a detecting device that combines a transducer with a biologically sensitive and selective component. Biosensors can measure compounds present in the environment, chemical processes, food and human body at low cost if compared with traditional analytical techniques. This book covers a wide range of aspects and issues related to biosensor technology, bringing together researchers from 12 different countries. The book consists of 20 chapters written by 69 authors and divided in three sections: Biosensors Technology and Materials, Biosensors for Health and Biosensors for Environment and Biosecurity.

How to reference

In order to correctly reference this scholarly work, feel free to copy and paste the following:

Maesoon Im and Yang-Kyu Choi (2011). Numerical Analysis and Simulation of Fluidics in Nanogap-Embedded Separated Double-Gate Field Effect Transistor for Biosensor, *New Perspectives in Biosensors Technology and Applications*, Prof. Pier Andrea Serra (Ed.), ISBN: 978-953-307-448-1, InTech, Available from: <http://www.intechopen.com/books/new-perspectives-in-biosensors-technology-and-applications/numerical-analysis-and-simulation-of-fluidics-in-nanogap-embedded-separated-double-gate-field-effect>

INTECH
open science | open minds

InTech Europe

University Campus STeP Ri
Slavka Krautzeka 83/A
51000 Rijeka, Croatia
Phone: +385 (51) 770 447
Fax: +385 (51) 686 166
www.intechopen.com

InTech China

Unit 405, Office Block, Hotel Equatorial Shanghai
No.65, Yan An Road (West), Shanghai, 200040, China
中国上海市延安西路65号上海国际贵都大饭店办公楼405单元
Phone: +86-21-62489820
Fax: +86-21-62489821

© 2011 The Author(s). Licensee IntechOpen. This chapter is distributed under the terms of the [Creative Commons Attribution-NonCommercial-ShareAlike-3.0 License](https://creativecommons.org/licenses/by-nc-sa/3.0/), which permits use, distribution and reproduction for non-commercial purposes, provided the original is properly cited and derivative works building on this content are distributed under the same license.

IntechOpen

IntechOpen